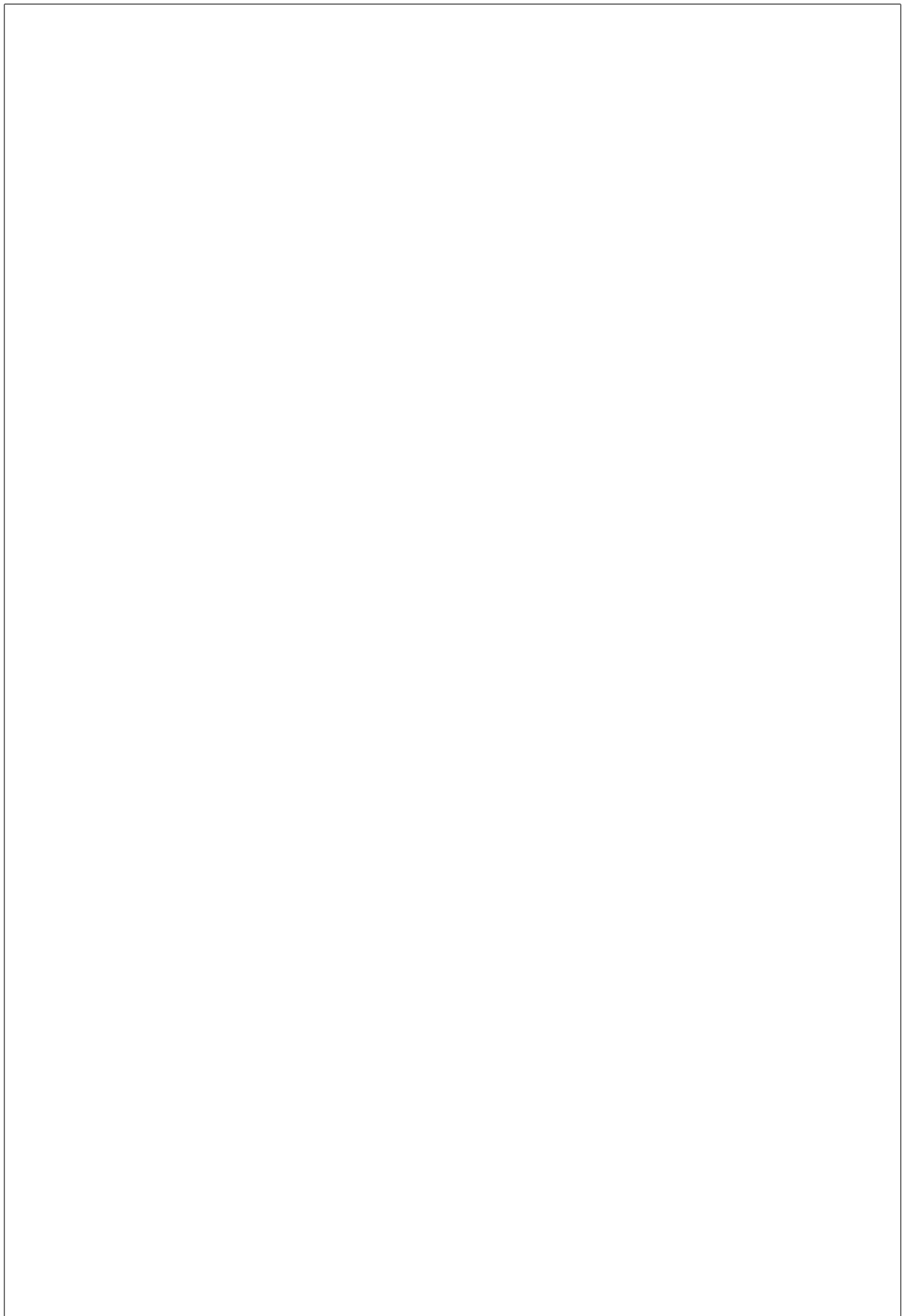


---

---



---

## Todo list

type . . . . . 3

---

---

# Contents

<b>Table of Contents</b>	i
<b>List of Tables</b>	i
<b>1 Quality of Nanodiamonds</b>	1
1.1 Quality-improving Post-Processing Treatments . . . . .	2
1.1.1 Annealing and Oxidation . . . . .	2
1.1.2 Surface Treatment With Gas And Plasma . . . . .	3
1.2 Raman Measurements . . . . .	3
1.2.1 Surface Contamination . . . . .	4
1.2.2 Defect Concentration . . . . .	5
1.2.3 Lattice Strain . . . . .	5
1.3 Transmission Electron Microscopy . . . . .	6
1.3.1 Crystallinity and Grain Boundaries . . . . .	6
<b>Bibliography</b>	9

---

---

---

## List of Tables

---

# Chapter 1

## Quality of Nanodiamonds

Carbon exists in a variety of crystalline and disordered structures, exhibiting three hybridizations,  $sp^3$ ,  $sp^2$ ,  $sp^1$ , see Figure 1.1. In its  $sp^3$  configuration, characteristic of diamond, each of the four carbon valence electrons are assigned to a tetrahedrally directed  $sp^3$  orbital resulting in strong  $\sigma$  bonds with adjacent atoms. In the three-fold coordinated  $sp^2$  configuration of graphite,  $\sigma$  bonds form a bonding plane as three of the four valence electrons participate in trigonally directed  $sp^2$  orbitals. The remaining fourth electron of the  $sp^2$  is found in a  $p_z(p\pi)$  orbital normal to the bonding plane. Here  $\pi$  orbital form weaker  $\pi$  bonds between one or more neighboring atoms. The final configuration is denoted  $sp^1$  where two out of four valence electrons enter  $\sigma$  orbitals. Here  $\sigma$  bonds are formed directed along the x-axis. The remaining two electrons participate in  $p\pi$  orbitals in the y and z directions. Strong directional  $\sigma$  bonds give rise to the extreme physical properties of carbon in its diamond form. Graphite is characterized by strong intra-layer  $\sigma$  bonding and weak van der Waals bonding across different layers [1].

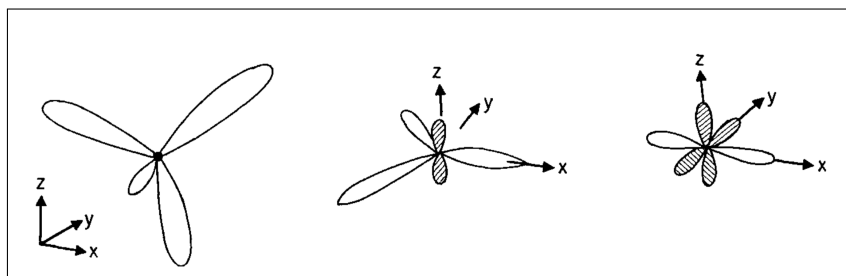


Figure 1.1: The  $sp^3$ ,  $sp^2$ ,  $sp^1$  hybridized bonding of carbon [2].

In this thesis we perform measurements of SiV centers hosted in nanodiamonds produced by various means ???. In this context we use the term quality as a measure of how close diamond crystals are to their pristine form. The presence of lattice imperfections such as additional vacancies, lattice strain, impurities or the inclusion of graphite or amorphous carbon is known to adversely affect crystal quality [3, 4, 5]. Surface contamination like graphite and amorphous  $sp^2$  hybridized carbon atoms man-

ifest themselves as additional peaks in the Raman spectrum. Strain in the diamond lattice broadens the first order Raman peak and causes it to shift to higher or smaller wavenumbers. Similarly, high concentrations of lattice defects cause additional peaks, a broadening of the first order Raman peak and a shift towards smaller wavenumbers. To improve crystal quality and to reduce the mentioned distracting effects the following methods are deployed here: Annealing in a vacuum, oxidation in air as well as surface treatments involving plasmas.

To study the effectiveness of these treatments and to gauge the quality of our nanodiamond samples we rely on Raman spectroscopy and TEM imaging. The former is used to detect strain, quantify defect concentration and the presence of carbon in non-diamond phases, while the latter enables imaging of individual nanodiamonds revealing details in crystallinity such as crystal boundaries.

## 1.1 Quality-improving Post-Processing Treatments

### 1.1.1 Annealing and Oxidation

In this thesis we perform measurements with nanodiamonds produced both by direct CVD growth and by wet-milling a CVD diamond film. In a chemical vapor deposition reactor, either an amorphous carbon deposit, or a crystalline diamond film may be produced depending on the ratio of the fluxes of carbon and atomic hydrogen onto a substrate [6, 7]. Hence, both the milled and directly grown nanodiamonds may be contaminated with amorphous carbon. The degree of contamination can be kept to a minimum by tuning the parameters of the growth process.

SiV centers were formed both via *in-situ* implantation during CVD growth and via silicon implantation. *In-situ* implantation disrupts the integrity of the diamond lattice and potentially leads to lattice damage. During silicon implantation the diamond lattice gets damaged by the penetrating ions.  $sp^2$  bonds, carbon interstitials and vacancies disrupt the metastable equilibrium of the diamond phase. Hence, there is a tendency for damaged diamond to “tip over” to the thermodynamically stable form of carbon, i.e. graphite.

At temperatures above about 500 °C, vacancies in the diamond lattice become mobile and diffuse towards the surface[8] disrupting the pristine diamond surface, causing surface contamination. Literature suggests, that annealing at 900 °C for 1 h is sufficient to remove most of the damage following implantations. To reduce the damage in the diamond lattice even further, we anneal the implanted diamonds at 900 °C to 1200 °C for 3 h to 6 h in vacuum ( $10^{-6}$  Pa).

The surface of the nanodiamonds is contaminated with graphite and amorphous  $sp^2$  hybridized carbon. In particular, for milled diamonds additional contaminations are commonly introduced by the milling process due to mechanical abrasions. To remove these, we apply oxidation in an oven under ambient air at a temperature of 450 °C for 3 h to 6 h.

### 1.1.2 Surface Treatment With Gas And Plasma

If contaminations are present on the surface of nanodiamonds they can absorb a fraction of the fluorescence light emitted from within the diamond. Thus they reduce the quantum yield of SiV centers. We want to explore the possibility of reducing the detrimental effects of surface contaminations via various surface treatments with different gases.

In particular, we treated our nanodiamonds with hydrogen ( $H_2$ ), oxygen ( $O_2$ ), ozone ( $O_3$ ) both at room temperature and at  $500^\circ C$ . Alternatively, we apply a  $H_2$  plasma<sup>1</sup>. Unfortunately, the only samples that yielded spectra with measurable ZPLs were the ones treated with  $H_2$ . However, we did not observe any luminescence enhancement. For all other treatments, we found that nanodiamonds either did not show any luminescence or immediately bleached upon excitation. Bleaching occurs even when using a continuous wave 660 nm laser at low excitation powers of  $200 \mu W$ . While we cannot say for sure why this is the case, we suspect that the treatments favor SiV center ionization. Since this approach did not seem fruitful, we did not pursue it further.

## 1.2 Raman Measurements

Raman spectroscopy of various samples gives insight into crystal quality and surface contamination of nanodiamonds. Raman scattering is the inelastic scattering of a photon  $\hbar\omega_i$  on a molecule or crystal lattice in the initial state  $|i\rangle$  with energy  $E_i$ . The molecule or crystal transitions into a higher energy state  $E_f$  and the scattered photon with frequency  $\omega_s$  loses the energy  $\Delta E = E_f - E_i = \hbar(\omega_i - \omega_s)$ . Therefore, energy is exchanged between the photon and the excited matter, changing the rotational or oscillation energy of the involved molecule or the oscillation energy, i.e. phonons of the crystal lattice. The Raman shift is typically referenced in wavenumbers and given by

$$\Delta\omega = \left( \frac{1}{\lambda_{ex}} - \frac{1}{\lambda_R} \right). \quad (1.1)$$

As every solid exhibits characteristic phonon modes tied to the properties of its lattice structure, Raman spectroscopy can be used to characterize diamond. Raman measurements of nanodiamonds give insight into the issues of surface contamination, lattice strain and defect concentration: Surface contamination like graphite and amorphous  $sp^2$  hybridized carbon atoms cause additional peaks in the Raman spectrum. A high defect concentration may lead to additional peaks, a broadening of the first order Raman peak and a shift to smaller wavenumbers. Strain in the diamond broadens the first order Raman peak and causes a shift to higher wavenumbers [3, 4, 5].

For Raman measurements the setup described in ?? is used. As excitation light source, a 532 nm continuous wave diode laser is used (IO ). It provides single frequency mode

<sup>1</sup>performed by O. Williams, School of Engineering, Cardiff University

type

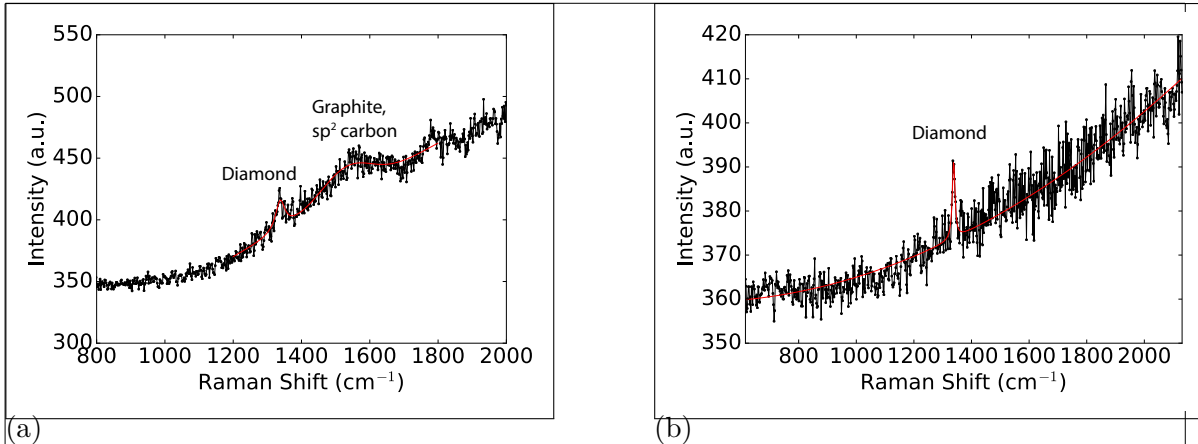


Figure 1.2: Raman measurements, black: data, red: fit. (a) Raman measurement before oxidation, sample insitu70. The diamond Raman peak is situated at  $1338\text{ cm}^{-1}$ . The broad feature around  $1580\text{ cm}^{-1}$  corresponds to the graphite G-band. (b) Raman measurement after oxidation, sample insitu70o. The G-band has vanished, indicating removal of graphite and amorphous  $\text{sp}^2$  hybridized carbon.

laser light, a prerequisite for Raman investigations. The beamsplitter is a dichroic mirror (DRLP645), the laser light is additionally blocked out with a 532 nm notch filter in the detection path in front of the single mode fiber replacing the usual long pass filter. With these adaptations, the combination of the confocal unit and the spectrometer serves as a Raman spectrometer. As the diamond Raman line is very narrow, the 600 grooves/mm grating does not offer sufficient resolution and is only used for a coarse approach. Detailed measurements are realized using 1200 grooves/mm and 1800 grooves/mm gratings.

Since the size of single nanodiamonds is on the order of tens of nanometers, low signal intensities can become an issue when taking Raman measurements. To overcome this problem we pursue two different approaches:

- Nanodiamond Clusters: Collective measurements are carried out at several areas on the sample insitu70. Since this sample is densely covered with nanodiamonds, collective measurements of clusters of nanodiamonds (??) achieve higher signal intensities.
- Big Nanodiamonds: Raman measurements are carried out on the implanted sample implanted250ao. For this sample, diamond particles are large enough to yield sufficient intensities on single nanodiamonds.

### 1.2.1 Surface Contamination

We test the impact of oxidation treatment as described in ?? on surface contamination. ?? shows a measured Raman spectrum of a sample without oxidation treatment

(insitu70n). To verify reproducibility, the measurement is performed on three different spots of the sample. The narrow peak in ?? corresponds to the first order diamond Raman peak and will be further analyzed in ?? . The spectrum also shows a broad peak with a Raman shift of about  $(1582 \pm 5) \text{ cm}^{-1}$ . This shift corresponds to the G-band due to amorphous  $\text{sp}^2$  hybridized carbon atoms and graphite. The exact G-band position and linewidth is sensitive to parameters such as the clustering of the  $\text{sp}^2$  phase, bond-length and bond-angle disorder, presence of  $\text{sp}^2$  rings or chains, and the  $\text{sp}^2/\text{sp}^3$  ratio [9]. The nanodiamond Raman spectra are considerably modified after oxidation in air at  $450^\circ\text{C}$ . To verify this, we perform Raman measurements on three different spots of a sample produced in the same process as the above mentioned, which is additionally oxidized (insitu70o). While the G-band peak is present in every measurement performed on a non-oxidized sample, it is not present in any of the oxidized samples (?? ), indicating successful removal of  $\text{sp}^2$  hybridized carbon and surface graphite.

### 1.2.2 Defect Concentration

Several effects impact the first order diamond Raman line: 1. defects in the diamond lattice, 2. hydrostatic pressure, 3. uniaxial or more complicated stress configurations. In the measurement on nanodiamond clusters the width of the diamond Raman peak of sample insitu70 varies between  $15 \text{ cm}^{-1}$  and  $30 \text{ cm}^{-1}$  without oxidation treatment, but is only  $9 \text{ cm}^{-1}$  to  $11 \text{ cm}^{-1}$  after the oxidation process. A possible reason for this change of the width is improved crystal quality [4]. In the measurement on big nanodiamonds we measured a Raman line at  $(1308 \pm 5) \text{ cm}^{-1}$  (denoted line R1) which exhibits a broad linewidth of  $(25 \pm 5) \text{ cm}^{-1}$ . One plausible explanation for both the position and the linewidth of the Raman line are defects in the diamond lattice[4].

### 1.2.3 Lattice Strain

We investigated how strain in the diamond lattice manifests itself in both measurements on nanodiamond clusters and on big nanodiamonds. In the Raman measurement on nanodiamond clusters, the position of the diamond Raman peak is the same for oxidized (insitu70o) and non-oxidized (insitu70n) samples, indicating that oxidation does not affect strain in the diamond. However, the Raman shift of both non-oxidized and oxidized samples amounts to  $(1338 \pm 5) \text{ cm}^{-1}$ , as compared to the literature value of  $1332.5 \text{ cm}^{-1}$  of pristine diamond [3] (given uncertainties are governed by spectrometer resolution). This shift indicates the presence of strain in the diamond particles.

Performing the Raman measurement on big nanodiamonds we found one diamond Raman line at  $(1308 \pm 5) \text{ cm}^{-1}$  (line R1), one at  $(1345 \pm 5) \text{ cm}^{-1}$  (line R2) and one at  $(1348 \pm 5) \text{ cm}^{-1}$  (line R3), indicating a broad distribution of strain among the individual diamond particles (uncertainties governed by spectrometer resolution). Only line R1 can be explained with a high defect concentration in the diamond lattice due to its shift to smaller wavelength. However, a more consistent model which explains all occurring shifts is the presence of strain in the diamond nano particles. From the linewidths

in the measurement on big nanodiamonds, the strain in the diamond is calculated using the equation for hydrostatic pressure [4] given by

$$\omega(P) = \omega_0 + a_1 P + a_2 P^2, \quad (1.2)$$

where  $\omega_0 = 1332.5 \text{ cm}^{-1}$ ,  $a_1 = 2.83 \text{ cm}^{-1} \text{ GPa}^{-1}$  and  $a_2 = -3.65 \times 10^{-3} \text{ cm}^{-1} \text{ GPa}^{-1}$ . The calculation yields a pressure in the investigated diamonds of  $-8.56 \text{ GPa}$  tensile stress and  $4.26 \text{ GPa}$  and  $5.50 \text{ GPa}$  compressive stress. Pressure uncertainties due to the Raman line measurements are smaller than one Pascal and are therefore neglected. Under hydrostatic pressure, the triply degenerate first order Raman peak remains degenerate, while under uniaxial and more complex stress configurations (biaxial stress, shear stress etc.) mode splitting occurs [4]. As mentioned above, we observe broad linewidths up to  $(25 \pm 5) \text{ cm}^{-1}$ . The broad linewidths of the Raman lines may be attributed to uniaxial strain, as mode splitting manifests itself in a broadening of the peak due to limited spectrometer resolution. Therefore, we conclude that both hydrostatic and uniaxial strain is present in the nanodiamonds.

## 1.3 Transmission Electron Microscopy

Transmission electron microscopy (TEM, also sometimes conventional transmission electron microscopy or CTEM) is a microscopy technique in which a beam of electrons is transmitted through a specimen to form an image. The specimen is most often an ultra-thin section less than  $100 \text{ nm}$  thick or a suspension on a grid. An image is formed through the interaction of the electrons with the sample as the beam is transmitted through the specimen. Since electrons have higher de Broglie wavelengths than photons, a higher resolution is obtainable, allowing the surface of nanodiamonds to be resolved. Thus, the crystallinity of single nanodiamonds can be studied directly.

### 1.3.1 Crystallinity and Grain Boundaries

For TEM investigations nanodiamond samples must obey certain size requirements. In particular, they must be large enough for the carbon grid inside the microscope acting as a stage for specimen to hold them. Furthermore, their diameter must not exceed a certain value, since the TEM electron beam must be able to permeate the material for imaging. Samples of type insitu100 mostly comprised of nanodiamonds fulfilling these requirements, was investigated by J. Schmauch, group of R. Birringer, Saarland University.

In ?? a TEM image of a single nanodiamond is shown. A complex crystal formation deviating from single crystal diamond structure is visible. A higher resolution detail is given in Figure 1.3b. The image clearly shows different crystal orientations, asserting that the nanodiamond particle is not a single crystal diamond. As a result, the imaged nanodiamond is of reduced crystal quality.

We have repeated this visual assessment of crystal quality for a range of different nanodiamonds with identical results. This supports the conclusion that all of our nanodiamonds are polycrystalline specimen.

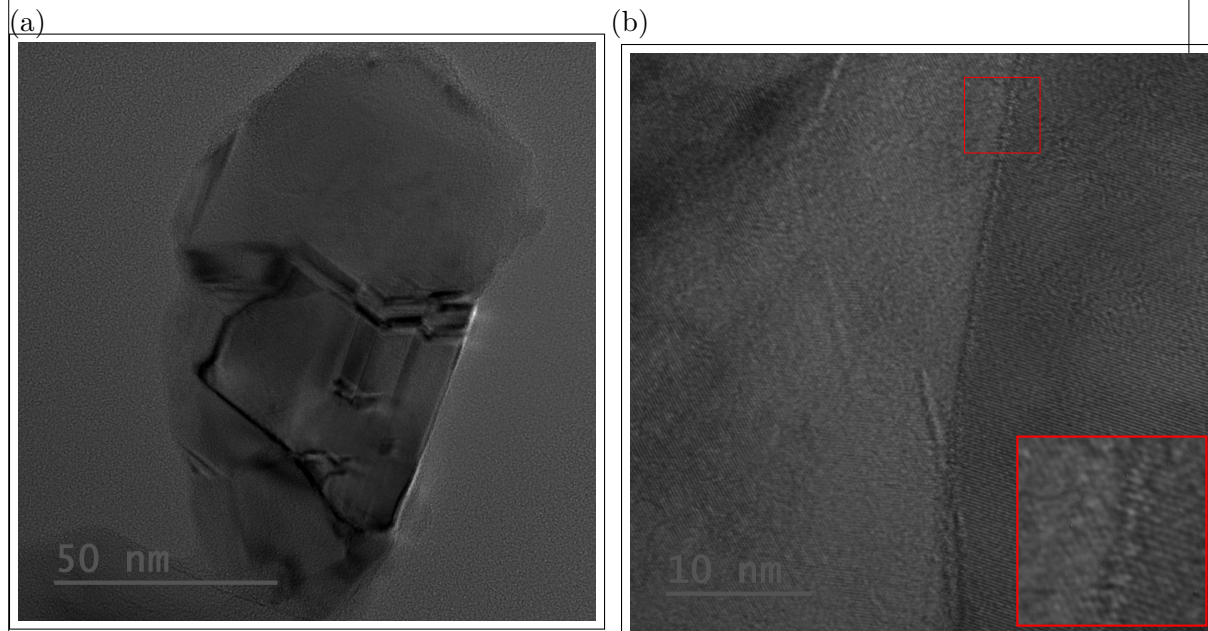
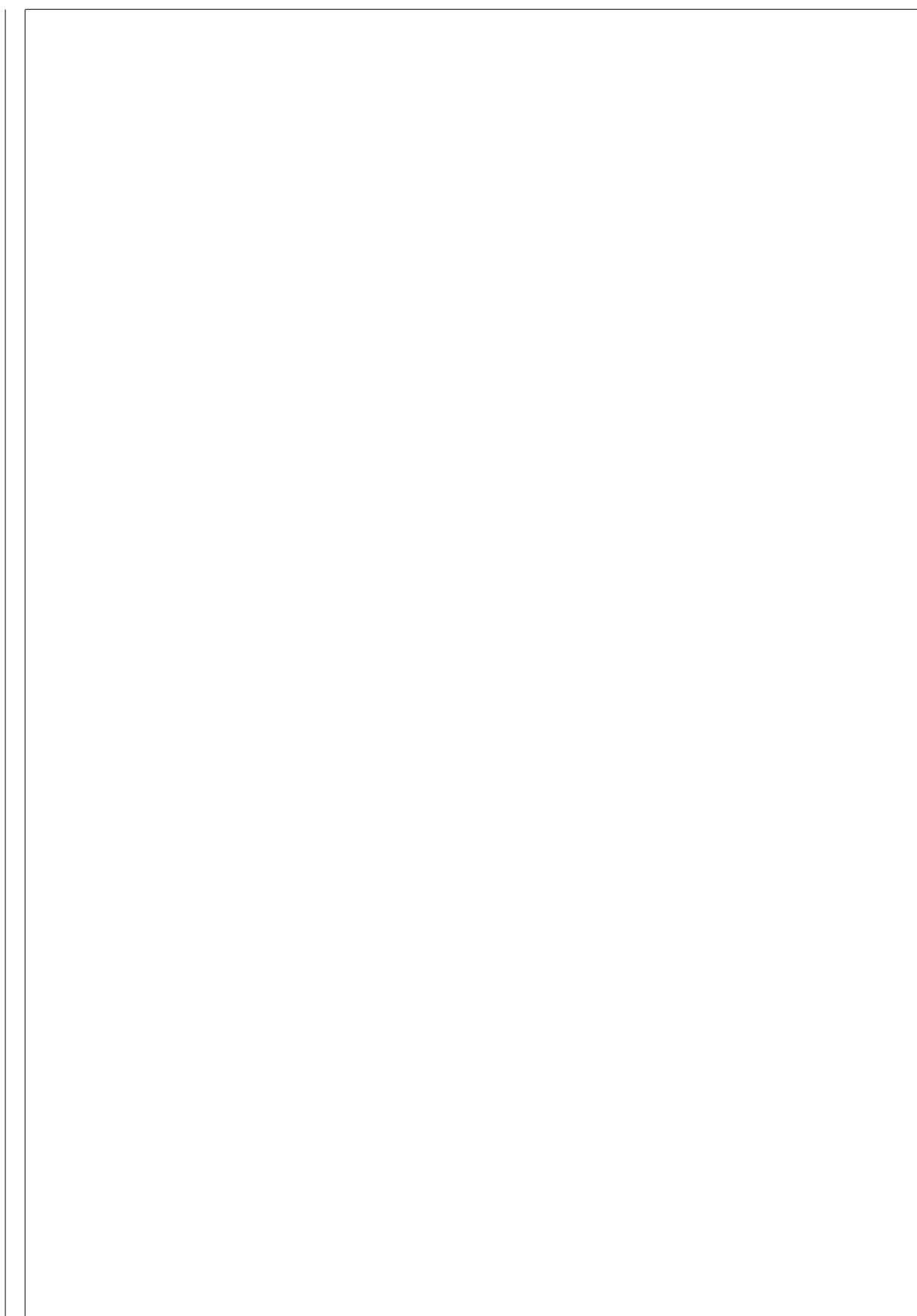


Figure 1.3: Transmission electron microscopy (TEM) pictures of sample insitu100. (a) Image of a single nanodiamond particle revealing a complex crystal structure. (b) Close-up image a diamond particle. The vertical line is a crystal boundary, to the left and right the parallel layers of one crystalline region can be seen. For better visibility, the inset shows a magnification of the area indicated by a red box. The different orientations of the crystal lattice layers is visible.



---

---

# Bibliography

- [1] J. Robertson. Diamond-like amorphous carbon. *Materials Science and Engineering: R: Reports*, 37(4-6):129–281, may 2002. 1
- [2] J Robertson. Advances in Physics Amorphous carbon. *Advances in Physics*, 35:317–374, 1986. 1
- [3] AM Zaitsev. *Optical properties of diamond: a data handbook*. 2001. 1, 3, 5
- [4] Steven Prawer and Robert J Nemanich. Raman spectroscopy of diamond and doped diamond. *Philosophical Transactions of the Royal Society A: Mathematical, Physical and Engineering Sciences*, 362(1824):2537–2565, nov 2004. 1, 3, 5, 6
- [5] J. O. Orwa, K. W. Nugent, D. N. Jamieson, and S. Prawer. Raman investigation of damage caused by deep ion implantation in diamond. *Physical Review B - Condensed Matter and Materials Physics*, 62(9):5461–5472, sep 2000. 1, 3
- [6] Ij Ford. Model of the Competitive Growth of Amorphous-Carbon and Diamond Films. 78(1):510–513, 1995. 2
- [7] Darin S. Olson, Michael A. Kelly, Sanjiv Kapoor, and Stig B. Hagstrom. Sequential deposition of diamond from sputtered carbon and atomic hydrogen. *Journal of Applied Physics*, 74(8):5167–5171, 1993. 2
- [8] M. S. Dresselhaus and R. Kalish. *Ion Implantation in Diamond, Graphite and Related Materials*, volume 22 of *Springer Series in Materials Science*. Springer Berlin Heidelberg, Berlin, Heidelberg, 1992. 2
- [9] Andrea Carlo Ferrari and John Robertson. Raman spectroscopy of amorphous, nanostructured, diamondâ€¢like carbon, and nanodiamond. *Philosophical Transactions of the Royal Society of London A: Mathematical, Physical and Engineering Sciences*, 362(1824):2477–2512, 2004. 5